


## Article

# Dynamic Response and Lubrication Performance of Spur Gear Pair Under Time-Varying Rotation Speeds

Jiaxing Pei <sup>1</sup>, Yuanyuan Tian <sup>2,\*</sup>, Hongjuan Hou <sup>1,\*</sup>, Yourui Tao <sup>3</sup>, Miaojie Wu <sup>4</sup>  and Zhigang Guan <sup>1</sup>

<sup>1</sup> School of Mechanical and Equipment Engineering, Hebei University of Engineering, Handan 056038, China; tbve\_kr@163.com (J.P.); grvigh-918@163.com (Z.G.)

<sup>2</sup> School of Mechanical and Aerospace Engineering, Nanyang Technological University, Singapore 639798, Singapore

<sup>3</sup> State Key Laboratory of Reliability and Intelligence of Electrical Equipment, Hebei University of Technology, Tianjin 300401, China; taoyourui@hebut.edu.cn

<sup>4</sup> College of Mechanical Engineering, Tianjin University of Technology, Tianjin 300401, China; wu\_miaojie@foxmail.com

\* Correspondence: yuanyuan.tian@ntu.edu.sg (Y.T.); houghongjuan@hebeu.edu.cn (H.H.)

**Abstract:** The rotation speed directly influences the vibration and lubrication behaviors of gear pairs, but studying the effects of time-varying rotation speeds during their operation poses substantial challenges. The present work proposed an approach to analyzing the dynamic response and lubrication performance of spur gear pairs under time-varying rotation speeds. A single-degree-of-freedom torsional dynamics model was established to capture the vibration responses and meshing forces of a gear pair, with the meshing stiffness modulated by the time-varying rotation speed. Additionally, a transient elasto-hydrodynamic lubrication model of the gear system was proposed to obtain the pressure profile and film shape, incorporating the effects of time-varying rotation speeds. Three types of time-varying rotation speeds were investigated: acceleration, deceleration, and oscillation. The results reveal that the time-varying rotation speed induces chaotic motion of the gear system, resulting in significant changes in the dynamic meshing force, entrainment velocity, and curvature radius of the gear pair compared to those in constant-speed scenarios. The lubrication performance under time-varying rotation speeds also shows diverse dynamic characteristics, highlighting significant differences from that observed under a constant rotation speed. These insights contribute to a more comprehensive understanding of gear dynamics under realistic operating conditions, enhancing gears' performance and reliability in practical applications.

**Keywords:** spur gear; time-varying rotation speed; dynamic response; transient elasto-hydrodynamic lubrication



Received: 4 December 2024

Revised: 20 December 2024

Accepted: 2 January 2025

Published: 3 January 2025

**Citation:** Pei, J.; Tian, Y.; Hou, H.; Tao, Y.; Wu, M.; Guan, Z. Dynamic Response and Lubrication

Performance of Spur Gear Pair Under Time-Varying Rotation Speeds.

*Lubricants* **2025**, *13*, 15.

<https://doi.org/10.3390/lubricants13010015>

**Copyright:** © 2025 by the authors. Licensee MDPI, Basel, Switzerland. This article is an open access article distributed under the terms and conditions of the Creative Commons Attribution (CC BY) license (<https://creativecommons.org/licenses/by/4.0/>).

## 1. Introduction

The gear system has many distinguished merits, such as high transmission efficiency, high transmission accuracy, and high reliability. Consequently, gear transmissions are used widely in mechanical equipment. Investigating gears has attracted a large number of researchers, and research on gear vibration and lubrication has always been important. The gear pair's vibration response is extremely complex, and it directly affects the smoothness and reliability of gear operation. The dynamic load caused by vibrations affects the formation of a lubricating oil film. Lubrication failure can increase the friction and wear and even result in tooth surface failure. Nevertheless, the dynamic response and lubrication

behaviors of certain gear systems with time-varying rotation speeds, such as wind turbine and robot reducer gears, is still not known clearly.

A gear transmission system is a typical nonlinear dynamics system, and the earliest gear dynamics analyses can be traced back to the 1920s and early 1930s [1]. After nearly 100 years of development, several methods and models have been developed for studying the vibration responses of gear pairs. Kahraman et al. [2] established a single-degree-of-freedom model that accounted for the backlash and static transmission error, but the time-dependent characteristics of the meshing stiffness were neglected. Chaotic and subharmonic resonances were observed in their study. Blankenship and Kahraman [3] studied the complex behavior of a vibration system with clearance through analytical and numerical methods, and a gear dynamics test rig was designed to verify the solutions. Kahraman and Blankenship [4] observed the nonlinear behavior of a gear pair considering the clearance and a periodically time-varying mesh stiffness function through experiments. Cheng et al. [5] established a dynamics model of a gear system which could consider the lubrication. Their conclusion revealed that the surface roughness played an important role in the meshing stiffness, damping, and gear performance. Wu et al. [6] proposed a gear dynamics analysis approach that accounted for the effect of tooth cracks. Specifically, the influence of tooth cracks on the engaged stiffness of the gear pair was considered. Yi et al. [7] proposed a nonlinear dynamics model of a gear system that accounted for the time-varying pressure angle and the backlash caused by bearing deformation. They found that the system might approach a chaotic state early. Shahmasoorian et al. [8,9] undertook a tremendous amount of work on chaos estimation for and control over nonlinear systems. Shi et al. [10] developed a gear dynamics model that included the effect of the tooth separation and the backside mesh. Cheng et al. [11] studied the impact of teeth wear on the dynamic characteristics of gears. They found that the wear of the teeth changed the meshing stiffness and meshing position and further impacted the dynamic response of the gear pair. Cao et al. [12] investigated the effect of the load on the meshing stiffness and developed a nonlinear dynamics model that accounted for the force-dependent meshing stiffness, backlash, and profile deviation. Hasnijeh et al. [13] studied the vibration behaviors of a spur gear system considering stochastic external excitations. From the above discussion, the time-varying mesh stiffness, backlash, static transmission error, and external load have been the focuses of gear dynamics research. The effects of these external and parametric excitations on the vibration responses of gear pairs have been studied systematically. However, the studies discussed above neglected the variations in the rotation speed, which play a crucial role in the meshing stiffness. The meshing stiffness is associated with the engagement position of the gear joint, and it is a periodic function of time when the rotation speed of the gears is constant. For this condition, the time for the gear pair to rotate by one tooth is fixed, and it is called the meshing cycle. However, in practice, the rotation speed of the gear does not always remain constant, such as in industrial robots and machine tools; the speed of a gear pair varies over time. The meshing stiffness is no longer periodic, with a constant period as a result. The meshing stiffness has to be converted from the space domain into the time domain based on the rotation speed. Khabou et al. [14] studied the dynamic behavior of gear sets powered by electric and four-cylinder diesel engines. The variations in the rotation speed and torque were considered in their work. However, the influence of a time-varying rotation speed was not investigated.

Elastohydrodynamic lubrication (EHL) is another significant field of gear research. The analysis approach to investigations of gear EHL has developed maturely. The current EHL model, which can account for factors including the temperature effect, surface roughness, non-Newtonian behavior of the lubricant, and transient effects, meets the engineering practice requirements. Li and Kahraman [15–17] studied the effect of transient and dynamic

behaviors on the lubrication performance of gear transmission. The surface roughness was considered in their works. As with surface roughness, the manufacturing errors is significant to the lubrication performance of gear systems. Hjelm and Wahlström [18] established a thermal elastohydrodynamic lubrication model which could take into account the manufacturing errors. The results revealed that manufacturing errors had a great influence on the lubrication behavior of the gear system. Xiao et al. [19] studied normal and tangential oil film damping of gears using a transient thermal EHL model. The non-Newtonian effect of the lubricant was also considered in their work. Jamali et al. [20] proposed a transient EHL model for point contact to consider the longitudinal crowning of the spur gear teeth. They found that the film thickness close to the tooth edges obviously increased. Liu and Gong [21] established a thermal EHL model for helical gears to investigate the influences of profile modifications, the input torque, and the rotation speed on the flash temperature. To study the lubrication characteristics of spur gears under transient impacts and vibration conditions, Huang et al. [22] proposed an EHL model that accounted for thermal and squeeze effects. The results revealed that the film temperature and pressure increased remarkably while the film thickness decreased. Yin et al. [23] studied the lubrication performance of double involute gears at the graded position of the tooth waist. They found the thermal effect had a negligible influence on the lubrication characteristics at this position. In summary, gear EHL has already been studied thoroughly. As is well known, the rotation speed, which affects the curvature radius, entrainment velocity, and contact force, is essential to the lubrication performance of gear pairs. The rotation speed of the gear pair has usually been assumed to be constant in previous studies. As discussed earlier, the rotation speed is not always constant. However, an EHL model and an analysis method for gear pairs with time-varying rotation speeds are still absent, and thus the lubrication characteristics of gear systems with time-varying rotation speeds remain unclear.

This work proposed an approach to studying the transient response and lubrication performance of spur gear pairs under time-varying rotation speeds. First, a nonlinear dynamics model of the gear system was established, incorporating the time-varying meshing stiffness, static transmission error, and backlash. The meshing stiffness model, based on the Ishikawa method, was developed by considering the variation in the rotation speed. Additionally, a transient EHL model for the gear pair was formulated to account for the dynamic changes in lubrication caused by variations in speed. Three types of rotation speeds of acceleration, deceleration, and oscillation were analyzed to assess their impacts on the gear dynamics and lubrication behavior. This study provides insights into the influence of time-varying rotation speeds on both the transient responses and lubrication characteristics of a spur gear pair, advancing our understanding of the gear performance under realistic operating conditions.

## 2. Materials and Methods

### 2.1. Time-Varying Stiffness

Several approaches are usually employed to obtain the meshing stiffness along the meshing line, and the Ishikawa approach was used in this work. As can be seen in Figure 1, the gear tooth is simplified as a combination of a rectangle and a trapezoid according to the Ishikawa method. The calculation process is shown in detail in Refs. [24,25]. The meshing stiffness under different rotational angles was ultimately obtained as follows:

$$k(\theta) = \frac{F_n}{\delta} \quad (1)$$

where  $k$  denotes the meshing stiffness, which is a function of the rotational angle. An

involute spur gear pair is employed in this paper, and its parameters are shown in Table 1; the meshing stiffness is obtained and is shown in Figure 2.

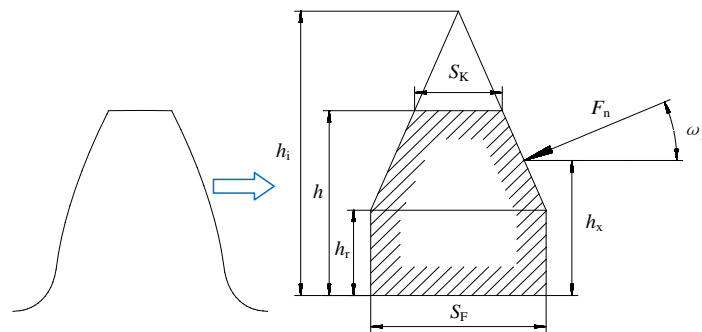


Figure 1. Approximate tooth profile using the Ishikawa method.

Table 1. Gear data.

Symbol, Unit	Gear Pair
Number of teeth, $z_1:z_2$	35:58
Pressure angle, $^\circ$	20
Module, mm	3
Face width, mm	20
Rotational inertia, $\text{kg}\cdot\text{mm}^2$	1860/13,590
Constant component of rotation speed, rad/min	2000
Center distance, mm	139.5
Modulus of elasticity, GPa	206
Damping ratio	0.05

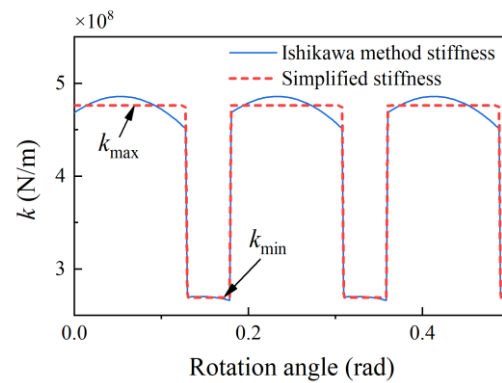


Figure 2. Meshing stiffness.

For simplicity, the meshing stiffness is translated into a square wave. The maximum stiffness is the mean of the double-tooth meshing region, and the minimum is the mean of the single-tooth area. The meshing stiffness and the simplified stiffness are depicted in Figure 2. The maximum and minimum values of the square wave stiffness are defined as follows:

$$k_{\max} = \frac{1}{\theta_d} \int_0^{\theta_d} k(\theta) d\theta \quad (2)$$

$$k_{\min} = \frac{1}{\theta_s} \int_{\theta_d}^{\theta_d + \theta_s} k(\theta) d\theta \quad (3)$$

where  $k_{\max}$  and  $k_{\min}$  represent the maximum and minimum square wave stiffness;  $\theta_d$  and  $\theta_s$  are the angular displacement in double-tooth and single-tooth meshing, and they can be defined as follow:

$$\theta_s = \theta_t(2 - \varepsilon) \quad (4)$$

$$\theta_d = \theta_t(\varepsilon - 1) \quad (5)$$

where  $\theta_t$  is the meshing angle of one tooth, which defines  $\theta_t = 2\pi/z$ , and  $\varepsilon$  is the contact ratio.

Three types of time-varying rotations are employed in this paper. The first and second types of rotation speed are acceleration and deceleration, respectively.

$$\dot{\theta} = \ddot{\theta}t \quad (6)$$

where  $\dot{\theta}$  is the rotation speed, and  $\ddot{\theta}$  denotes the acceleration of the rotation speed; if  $\ddot{\theta}$  is negative, this corresponds to deceleration.

The third type is a harmonic function of time, which can be expressed as follows:

$$\dot{\theta} = \dot{\theta}_c + A \sin(\omega_r t + \varphi_r) \quad \omega_r = 2\pi n_1/60 \quad (7)$$

where  $\dot{\theta}_c$  denotes the constant component of the rotation speed,  $A$  represents the amplitude of varying components,  $\omega_r$  is the angular frequency, and  $\varphi_r$  denotes the phase angle. If the initial rotation angle is zero, the rotation angle can be calculated as follows, respectively:

$$\theta = \dot{\theta}t + \frac{\ddot{\theta}t^2}{2} \quad (8)$$

$$\theta = \dot{\theta}_c t + \frac{A}{\omega_r} [1 - \cos(\omega_r t + \varphi_r)] \quad (9)$$

Based on Equations (5) and (6), the engaged stiffness is a time function.

$$k(t) = \begin{cases} k_{\max}, & (i+1-\varepsilon)\theta_t < \theta < i\theta_t \\ k_{\min}, & \text{else} \end{cases} \quad (10)$$

where  $i$  is the cycle number. The gear meshing stiffness model can consider time-varying rotation speeds. The meshing stiffness can easily transform from the space domain to the time domain regardless of the form of the time-varying speed.

## 2.2. The Dynamics Model of the Gear Pair

A gear pair is a strong nonlinear dynamics system, and several typical nonlinear phenomena, such as chaos and jump discontinuities, exist in gear dynamic systems. These nonlinear phenomena mainly originate from the time-variant mesh stiffness and backlash. The rotation speed plays an important role in the time-varying meshing stiffness. A torsional dynamic model is developed to investigate the influence of the time-dependent speed on the dynamic behavior of the gear system. As illustrated in Figure 3, the pinion and gear are considered as two rigid disks with corresponding masses. The contact of the tooth is replaced by a massless spring and massless damping. The kinetics model can include the backlash and static transmission error. According to Newton's law, a dynamics equations can be obtained [26]:

$$\begin{cases} I_1 \ddot{\theta}_1 + R_{b1}c(R_{b1}\dot{\theta}_1 - R_{b2}\dot{\theta}_2 - \dot{e}) + R_{b1}k(t)(R_{b1}\theta_1 - R_{b2}\theta_2 - e) = T_1 \\ I_2 \ddot{\theta}_2 + R_{b2}c(R_{b1}\dot{\theta}_1 - R_{b2}\dot{\theta}_2 - \dot{e}) - R_{b2}k(t)(R_{b1}\theta_1 - R_{b2}\theta_2 - e) = T_2 \end{cases} \quad (11)$$

where  $I_i$  is the rotary inertia,  $\theta_i$  is the torsional angular displacement,  $R_{bi}$  denotes the base cycle radius of the gear, and  $i = 1, 2$  are the pinion and the gear, respectively.  $T_1$  and  $T_2$  are

the input and output torque, and  $e$  denotes the transmission error due to manufacturing.  $k(t)$  represents the mesh stiffness, which is time-varying.  $c$  denotes constant viscous damping:

$$c = 2\zeta\sqrt{m_e k_m} \tag{12}$$

where  $\zeta$  represents the damping ratio,  $m_e$  denotes the equivalent mass of the gear system, and  $k_m$  is the average mesh stiffness.

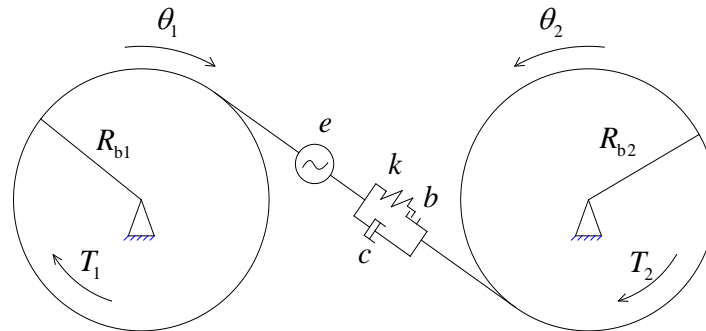


Figure 3. Dynamics model of gear system.

Let  $x = R_{b1}\theta_1 - R_{b2}\theta_2 - e$ ; Equation (11) can be rewritten as follows [26]:

$$m_e\ddot{x} + c\dot{x} + k(t)g(x) = f - m_e \frac{d^2e}{dt^2} \tag{13}$$

in which

$$m_e = \frac{I_1 I_2}{I_1 R_{b2}^2 + I_2 R_{b1}^2} \tag{14}$$

$$g(x) = \begin{cases} x - b, & x > b \\ 0, & -b \leq x \leq b \\ x + b, & x < -b \end{cases} \tag{15}$$

$$f = \frac{T_1}{R_{b1}} = \frac{T_2}{R_{b2}} \tag{16}$$

where  $g(x)$  is the nonlinear displacement function.  $b$  is the backlash. The static transmission error is assumed to be sinusoidal [26]:

$$e = e_r \sin(\omega_e t + \varphi_e) \tag{17}$$

where  $e_r$  represents the amplitude;  $\omega_e$  denotes the angular frequency;  $\varphi_e$  represents the phase angle.

Based on the dimensionless variables and parameters below,  $X = x/b$ ,  $\omega_n = 2\zeta\sqrt{k_m/m_e}$ ,  $K = k/k_m$ ,  $F = f/(bk_m)$ ,  $T = t\omega_n$ ,  $\Omega_e = \omega_e/\omega_n$ ,  $F = e_r/b$ . The dimensionless form of Equation (14) can be written as follows:

$$\ddot{X} + 2\zeta\dot{X} + KG(X) = F + F_a\Omega_e^2 \sin(\Omega_e T + \varphi_e) \tag{18}$$

$$G(X) = \begin{cases} X - 1, & X > 1 \\ 0, & -1 \leq X \leq 1 \\ X + 1, & X < -1 \end{cases} \tag{19}$$

The time-varying rotation speed mainly affects the meshing stiffness. The meshing stiffness is no longer a function of time with a fixed period. The advantage of this model is

that it can be used to tackle dynamic response problems for a gear pair with any form of time-varying rotation speed.

The meshing force on the tooth can be calculated according to the dynamic response and the meshing stiffness:

$$f_t = k_i g(x) + c\dot{x} \quad (20)$$

### 2.3. Geometry and Kinematics Analysis

According to EHL theory, the contact of the gear teeth can be treated as the contact between a plane and a cylinder. The radius of the cylinder defines the equivalent radius which can be obtained using the geometry analysis. The curvature radii of the two gear teeth at the contact point can be expressed as follows:

$$R_1 = R_{b1} \tan(\theta_0 + \theta_{mi}) \quad (21)$$

$$R_2 = s_2 - (R_1 - s_1) \quad (22)$$

where  $\theta_0$ ,  $s_1$ ,  $s_2$  are the geometry parameters displayed in Figure 4.  $\theta_{mi}$  is the rotation angle of the  $i$ th tooth, which changes from zero to  $\theta_i$ .  $\theta_i$  is the rotation angle of the  $i$ th tooth from the approach point to the recession point. The curvature radii can be transformed into the time domain with the known gear rotational speed. With the curvature radii of the contact teeth, the equivalent radius can be obtained [18]:

$$R = \frac{R_1 R_2}{R_1 + R_2} \quad (23)$$

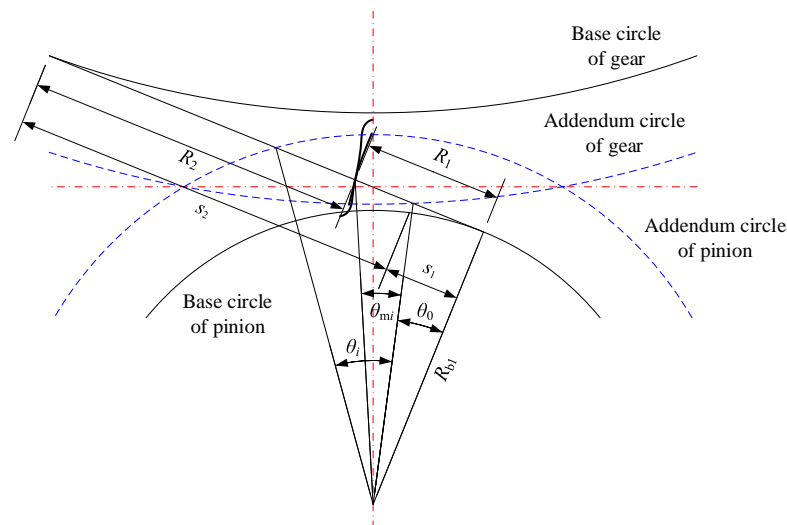


**Figure 4.** Geometric size of gear system.

The transient tangential velocity of the teeth at the contact point can be expressed as follows [27]:

$$u_1 = \dot{\theta}_1 R_1 \quad (24)$$

$$u_2 = \dot{\theta}_2 R_2 \quad (25)$$

where  $\dot{\theta}_1$  and  $\dot{\theta}_2$  are the rotation speed of the gear and the pinion, respectively. The entrainment velocity can be written as follows:

$$u = \frac{u_1 + u_2}{2} \quad (26)$$

where  $u_1$  and  $u_2$  are the rolling speeds of the teeth at the contact point, respectively.

#### 2.4. The Transient EHL Model

A lubricant film forms in the contact region of the teeth. The pressure of the lubricant film is controlled by the Reynolds equation. When the thermal effect is neglected, the line contact Reynolds equation for Newtonian fluid reads as follows [27]:

$$\frac{\partial}{\partial x} \left( \frac{\rho h^3}{\eta} \frac{\partial p}{\partial x} \right) = 12u \frac{\partial}{\partial x} (\rho h) + \frac{\partial}{\partial t} (\rho h) \quad (27)$$

where  $x$  represents the coordinate along the rolling direction;  $p$  denotes the hydrodynamic pressure;  $h$  represents the film's thickness;  $\rho$  and  $\eta$  represent the density and viscosity of the lubricant, respectively; and  $t$  represents the time.

The boundary and cavitation conditions should be known when solving the Reynolds equation, which define the following:

$$\begin{cases} x = x_0, p = 0 \\ x = x_e, p = \frac{\partial p}{\partial x} \Big|_{x=x_e} = 0 \end{cases} \quad (28)$$

where  $x_0$  and  $x_e$  are, respectively, the inlet and outlet locations of the lubricant.

The film thickness equation reads as follows [27]:

$$h(x) = h_0 + \frac{x^2}{2R} - \frac{4}{\pi E} \int_{x_0}^{x_e} p(s) \ln|x-s| ds \quad (29)$$

where  $h_0$  denotes the rigid body displacement, and  $E$  denotes the composite Young's modulus, which can be expressed as follows [18]:

$$\frac{1}{E} = \frac{1}{2} \left( \frac{1 - \nu_1^2}{E_1} + \frac{1 - \nu_2^2}{E_2} \right) \quad (30)$$

The equilibrium equation reads as follows:

$$w = \int_{x_0}^{x_e} p(x) dx \quad (31)$$

The Dowson–Higginson equation and the Roelands equation are employed to describe the relation of density and viscosity to pressure, respectively [28].

$$\rho = \rho_0 \left( 1 + \frac{0.6p}{1 + 1.7p} \right) \quad (32)$$

$$\eta = \eta_0 \exp \left\{ (\ln \eta_0 + 9.67) [-1 + (1 + 5.1 \times 10^{-9} p)^Z] \right\} \quad (33)$$

where  $\rho_0$  and  $\eta_0$  represent the density and viscosity of the lubricant in ambient conditions;  $Z$  denotes the viscosity–pressure index and is set to 0.68 in this paper [29,30].

A lack of dimensions can reduce the number of parameters and simplify the control equations. Hence, the following parameters are introduced to obtain a dimensionless form of the control equations.

$$X = \frac{x}{b_0}, H = \frac{hR_0}{b_0^2}, P = \frac{p}{P_H}, \bar{\eta} = \frac{\eta}{\eta_0}, \bar{\rho} = \frac{\rho}{\rho_0} \quad (34)$$

$$T = \frac{tu_s}{b_0}, P_H = \frac{Eb_0}{4R_0}, b_0 = \sqrt{\frac{8w_0R_0}{\pi E}}, U = \frac{u}{u_s}, \varepsilon = \frac{\bar{\rho}H^3}{\bar{\eta}\lambda}, \lambda = \frac{12\eta_0u_sR_0^2}{P_Hb_0^3} \quad (35)$$

where  $b_0$  represents the half-width of the Hertz contact region at the approach point of the



teeth;  $R_0$  is the equivalent radius at the approach point;  $P_H$  donates the maximum Hertz pressure of the approach point of contact of the teeth;  $u_s$  is the rolling speed of the approach point of contact of the teeth when the gear rotation speed corresponds to deceleration or sinusoidal variation, and the rolling speed of the recession point when the gear rotation speed corresponds to acceleration;  $w_0$  represents the force on a unit width of the gear tooth at the approach point.

The dimensionless forms of the Reynolds equation, the film thickness equation, and the equilibrium equation are defined as follows:

$$\frac{\partial}{\partial X} \left( \varepsilon \frac{\partial P}{\partial X} \right) = U \frac{\partial \bar{\rho} H}{\partial X} + \frac{\partial \bar{\rho} H}{\partial T} \quad (36)$$

$$H = H_{00} + \frac{X^2 R_0}{2R} - \frac{R_0}{\pi R} \int_{x_0}^{x_e} P(S) \ln|X - S| dS \quad (37)$$

### 2.5. The Numerical Procedure

Varying rotation speeds mainly impact the mesh stiffness of the gear system. Obtaining the mesh stiffness is the first step of a dynamics and lubrication analysis. The meshing stiffness along the line of action is calculated using the Ishikawa approach. The meshing stiffness is transformed into the time domain according to the time-varying rotation speed. A dynamics model of the gear system considering time-varying rotation speeds is proposed. The fourth-order Runge–Kutta method is employed for the solution of the dynamics equations. Then, the meshing force can be obtained according to the transient response of the gear pair. The curvature radii and the entrainment velocity are obtained through a geometry and kinematics analysis of the gear system. The transient EHL model is established to obtain the film thickness profile and the pressure distribution. The meshing time of each tooth is not equal. The number of discrete points is also unequal in each meshing cycle period. The inlet and outlet positions of the lubricant are  $x_0 = -4$  and  $x_e = 1.5$ , and 512 nodes exist in the  $X$  direction. The pressure and the film thickness from the previous time step are employed to initialize the current time step. The pressure and film thickness at the approach point are the solutions for the steady state. The pressure is Hertz pressure when the speed of the gear is equal to zero. The Gauss–Seidel iterative method is employed to obtain the pressure in light-load regions, and the Jacobi dipole iterative method is used in high-load regions. The iteration ends and proceeds to the next time step when the convergence criteria for the pressure and load are both satisfied. The convergence criteria are defined as follows:

$$\frac{\sum |p_i^{n+1} - p_i^n|}{\sum p_i^{n+1}} \leq \varepsilon_p \quad (38)$$

$$\frac{\left| \int_{x_0}^{x_e} p(x) dx - \pi/2 \right|}{\pi/2} \leq \varepsilon_w \quad (39)$$

where  $\varepsilon_p$  and  $\varepsilon_w$  are the thresholds for the relative error in the pressure and load; we take  $\varepsilon_p = 10^{-5}$  and  $\varepsilon_w = 10^{-3}$  in this paper. The equation was solved in this article using MATLAB R2021a.

## 3. Results and Discussions

Three types of time-varying rotation speeds are investigated in this paper. The first type of speed accelerates from zero to 200 rad/s at constant acceleration. The second decelerates from 200 rad/s to zero at constant deceleration. The third is the sum of a

constant speed and a sinusoidal wave. The amplitude of the sinusoidal wave is 0.5 times of the constant speed, and the frequency is the same as the pinion's rotation.

The parameters of the gear pair and the lubricant are summarized in Table 1. The types of time-varying rotation speeds and corresponding time-varying meshing stiffnesses are shown in Figures 5–7. The meshing stiffness is obtained using the model proposed in Section 2.1. The gears' rotation speed has a significant effect on the meshing stiffness. No periodicity exists in the meshing stiffness when the rotation speed corresponds to acceleration or deceleration. As depicted in Figure 5b, the meshing stiffness is simplified as a square wave; the lower edge of the square wave is a single-tooth mesh region, and the higher edge is a double-tooth mesh region. The tooth mesh cycle decreases as the rotation speed increases. Figure 7b demonstrates the meshing stiffness when the gear's rotation speed is sinusoidal. The meshing stiffness shows regular changes in density. The red lines in Figures 5–7 denote the meshing cycles selected for studying the following lubrication performance of the gear pair.

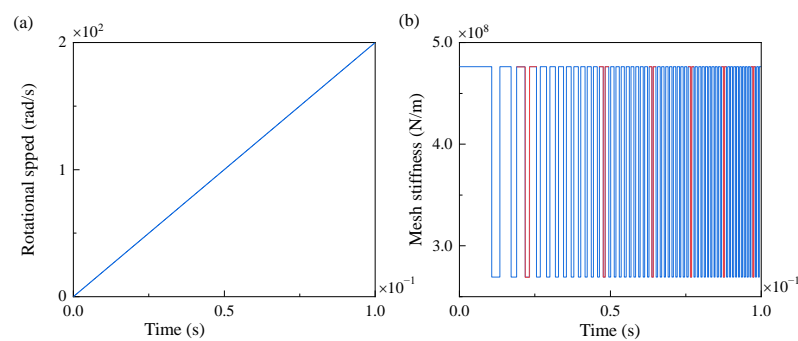


**Figure 5.** Acceleration and corresponding meshing stiffness: (a) rotational speed, (b) meshing stiffness.

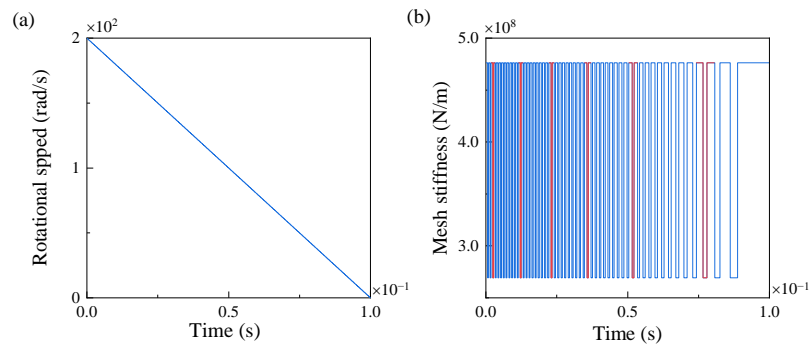


**Figure 6.** Deceleration and corresponding meshing stiffness: (a) rotational speed, (b) meshing stiffness.

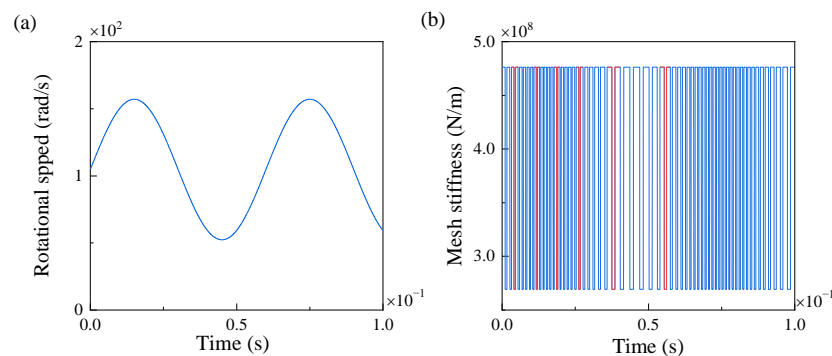


**Figure 7.** Sinusoidal rotational speed and corresponding meshing stiffness: (a) rotational speed, (b) meshing stiffness.

### 3.1. Dynamic Response of the Gear System with Time-Varying Rotation Speeds

The transient displacement of the gear pair with different types of rotation speed is shown in Figure 8. The dynamic response is obtained by solving the dynamics model for the gear pair. As can be seen, the response is more complex than the response of a constant-rotation-speed gear pair. No evident period is observed in the dynamic response. Severe fluctuation appears when the teeth enter into meshing and then gradually disappears. Fluctuation also appears when the number of teeth engaged changes. These fluctuations are the transient response of the gear pair, and the frequency is close to the natural frequency of the system. As shown in Figure 8a,b, the transient response is followed by a steady response. The fluctuation in the steady response regions is caused by the static transmission error, which is an internal excitation with a high frequency. The backlash is taken as  $10^{-4}$  m in this paper, so the teeth are always stay in contact, and no impact occurs. The other fluctuation is caused by time-varying meshing stiffness, and its frequency is not constant. The frequency increases with the rotation speed.

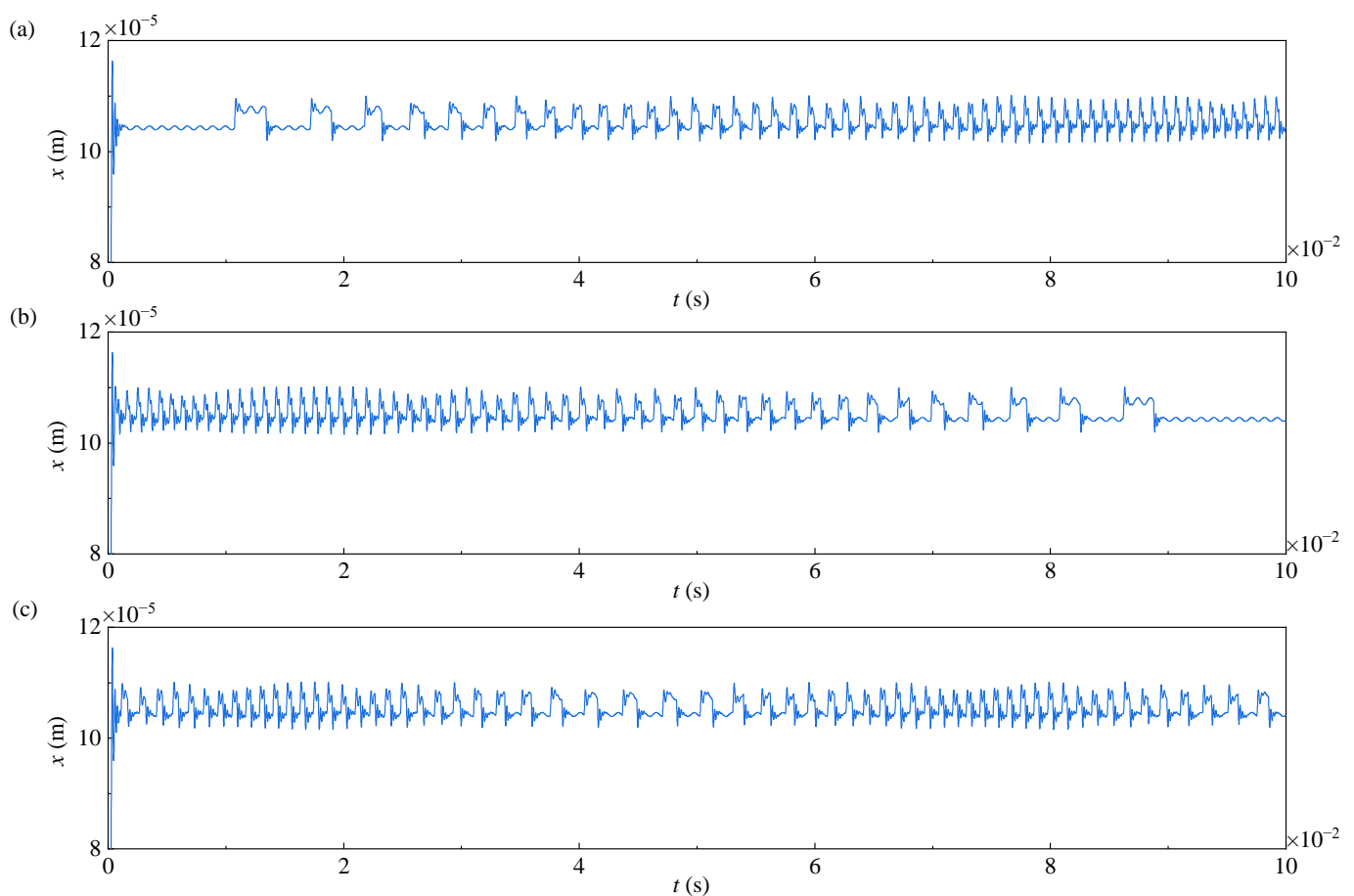


**Figure 8.** Dynamic response of gear pair with time-varying rotation speeds: (a) acceleration, (b) deceleration, and (c) sin form.

The Fourier spectra of the dynamic transmission error shown in Figure 9a–c correspond to acceleration, deceleration, and a sinusoidal rotation speed, respectively. As can be seen, rich frequency content exists in the amplitude-frequency spectrum. The conclusion can be drawn that the motions of the three rotational speeds are all chaotic. The amplitude–frequency spectra for acceleration motion and deceleration motion are essentially identical. The amplitude–frequency spectrum for a sinusoidal rotation speed is rougher. The gear system is more likely to enter into chaotic motion when the rotation speed is time-varying.

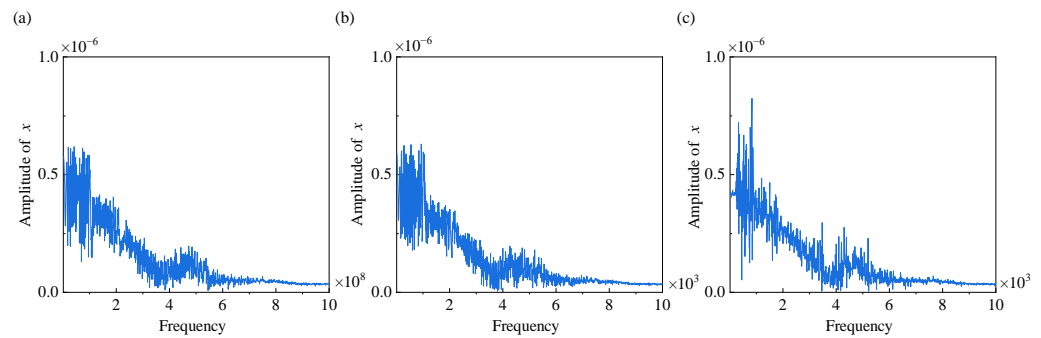


**Figure 9.** Fourier spectra of gear pair with time-varying rotation speeds: (a) acceleration, (b) deceleration, and (c) sin form.

### 3.2. Effect of Time-Varying Rotation Speeds on Gear Lubrication

Compared to the transmitted torque, the rotation speed plays a more significant role in the formation of the film of gear lubrication. The transmitted torque affects the dynamic meshing force, while the rotation speed also affects the curvature radius and the entrainment velocity. The curvature radius and the entrainment velocity in the third, fourth, and fifth stages of the acceleration process are illustrated in Figure 10. The curvature radius, entrainment velocity, and meshing force in each tooth meshing cycle are different when the rotation speed is time-varying. Figure 10a shows the curvature radii in different tooth meshing cycles. The values for the curvature radius from the approach point to the recession point are equivalent. However, the meshing time for each tooth is different. For the acceleration process, the meshing time is decreased. A trend can also be seen in Figure 10b for the entrainment velocity in different tooth meshing cycles. Unlike the curvature radius, the value of the entrainment velocity is different in each tooth meshing cycle. During the acceleration process, the entrainment velocity increases with time. This is because the entrainment velocity is positively correlated with the rotation speed. Figure 11 depicts the engagement force of the third to the fifth tooth. Fluctuation is also observed when the number of teeth engaged changes. The transient response disappears, and a steady-state response is entered. The frequency of the steady-state response is the same as the static transmission error. The engagement force in the single-tooth mesh region is larger than that in the double-tooth mesh regions. The contact area of the meshing teeth is related to the meshing force. So, the contact area for each tooth is different due to the meshing force on each tooth varying when the rotation speed is time-varying. The curvature radius, entrainment velocity, and engagement force on the tooth in the deceleration process and with a sinusoidal rotation speed also demonstrate different characteristics compared with those at a constant rotation speed. The Dowson and Higginson's (D-H) formula for the minimum film thickness is employed to validate the proposed model. The 15th tooth's meshing cycles at a sinusoidal rotation speed are selected. As shown in Figure 12, the minimum film thickness obtained using the present model is slightly smaller than that with the D-H formula. This is because the D-H formula neglects the transient effects.

Considering the complex calculation of the EHL simulation, six tooth meshing cycles of each type of time-varying speed are selected. For the acceleration and deceleration processes, the 3rd, 13th, 23rd, 33rd, 43rd, and 43rd tooth meshing cycles are chosen. For a sinusoidal rotation speed, the 3rd, 9th, 15th, 21st, 27th, and 33rd tooth meshing cycles are selected. The selected meshing cycles are highlighted in red in Figures 5–7. The dimensionless pressure and the film thickness distribution in the third engagement cycle of the acceleration process are depicted in Figure 13. The typical characters of EHL line contact, such as the quadratic pressure spike and the neck of the film thickness, are displayed at each time point. The pressure profile and the film distribution exhibit fluctuations caused

by the meshing force along the time axis. The trend is the same for the meshing force. The pressure in the engaged single-tooth region is larger, and the film thickness is thinner than that in the double-tooth meshing regions.

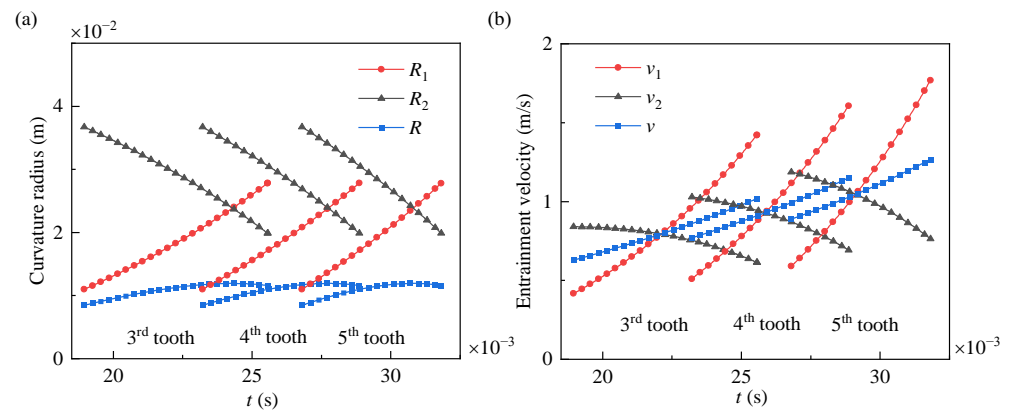


**Figure 10.** Curvature radius and entrainment velocity in different tooth meshing cycles in the acceleration process: (a) curvature radius and (b) entrainment velocity.

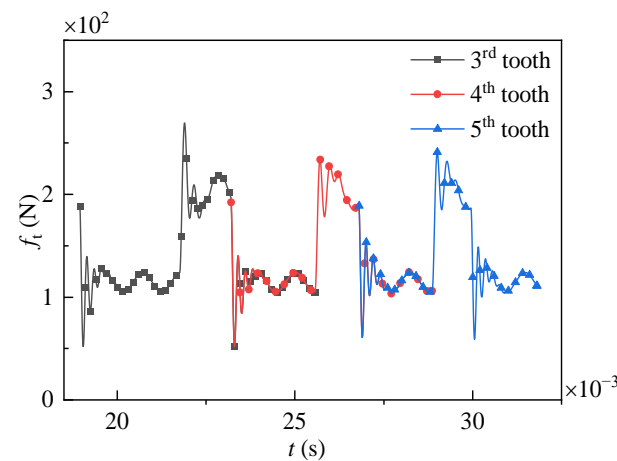


**Figure 11.** Meshing force in different meshing cycles of the acceleration process.

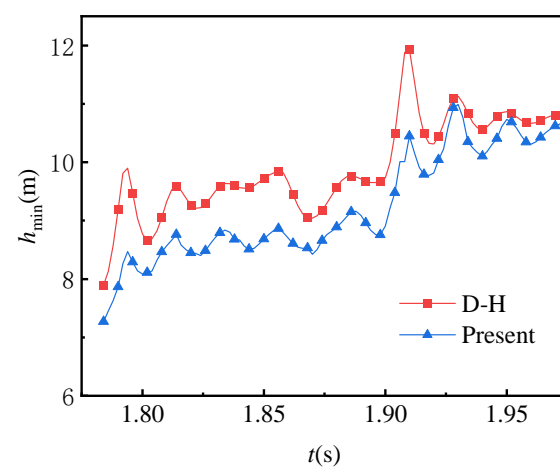


**Figure 12.** The minimum film thickness obtained using the D-H formula and the present model.

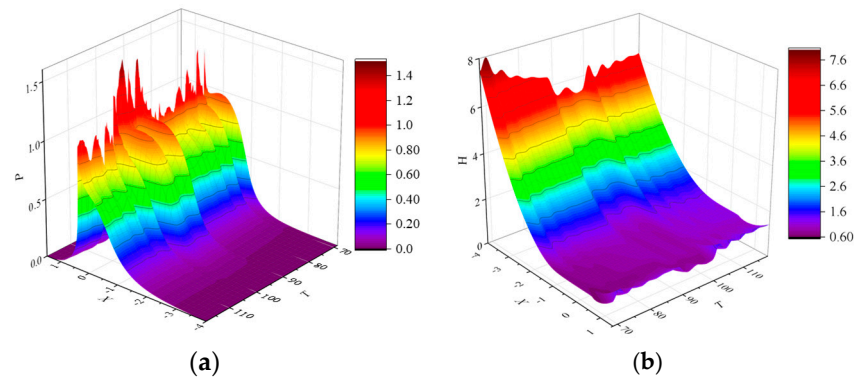


**Figure 13.** The pressure and film of the 3rd tooth from mesh-in to mesh-out in the acceleration process: (a) pressure profile and (b) film distribution.

The dimensionless minimum and central film thicknesses under three types of rotation speed are depicted in Figures 14–16. Figure 14 demonstrates the minimum and central film thicknesses in different meshing cycles of the acceleration process. The minimum and central film thickness both increase from mesh-in to mesh-out. The film thickness in different meshing cycles increases with an increasing rotation speed. Hence, the wear of the gear pair is more serious at the starting stage. Fluctuations exist in both the minimum and central film thicknesses, and the frequency is identical to the meshing force. As discussed previously, the meshing force on the tooth has two dominant frequencies: the higher frequency is the natural frequency of the system, and the lower frequency is caused by the static transmission error. The two frequencies are constant, and the tooth meshing cycle in the acceleration process decreases. So, the number of fluctuations decreases as the rotation speed increases. The range of fluctuations in the minimum film thickness is greater than that for the central film thickness. The high-frequency component is less obvious in the central film thickness. The film thickness in the engaged single-tooth region is thinner than that in the double-tooth meshing regions. The minimum film thickness suddenly increases when single-tooth meshing changes to double-tooth meshing. The minimum and central film thicknesses in different meshing cycles of the deceleration process are depicted in Figure 15. The film thickness decreases with a decreasing rotation speed. The film thicknesses in different meshing cycles increase from mesh-in to mesh-out. Nevertheless, they decrease as the rotation speed decreases.

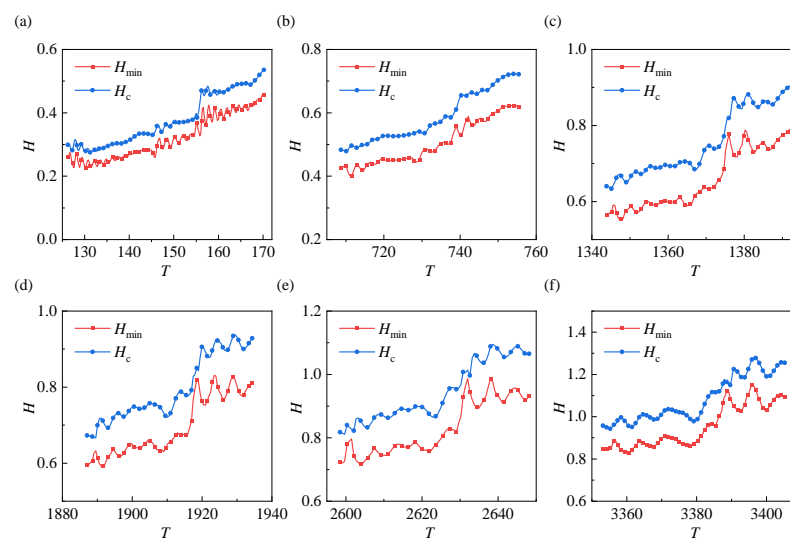


**Figure 14.** The minimum and central film thicknesses in different meshing cycles of the acceleration process (a–f) six different meshing cycles.

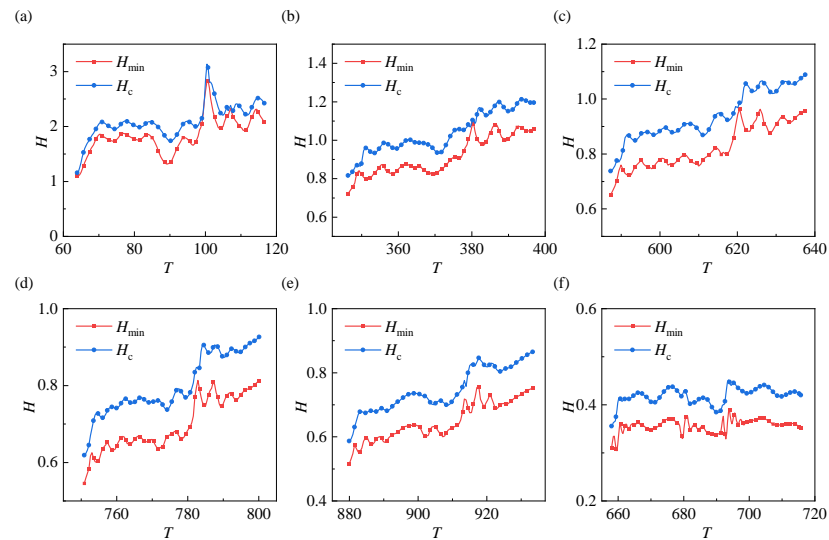


**Figure 15.** The minimum and central film thicknesses in different meshing cycles of the deceleration process (a–f) six different meshing cycles.

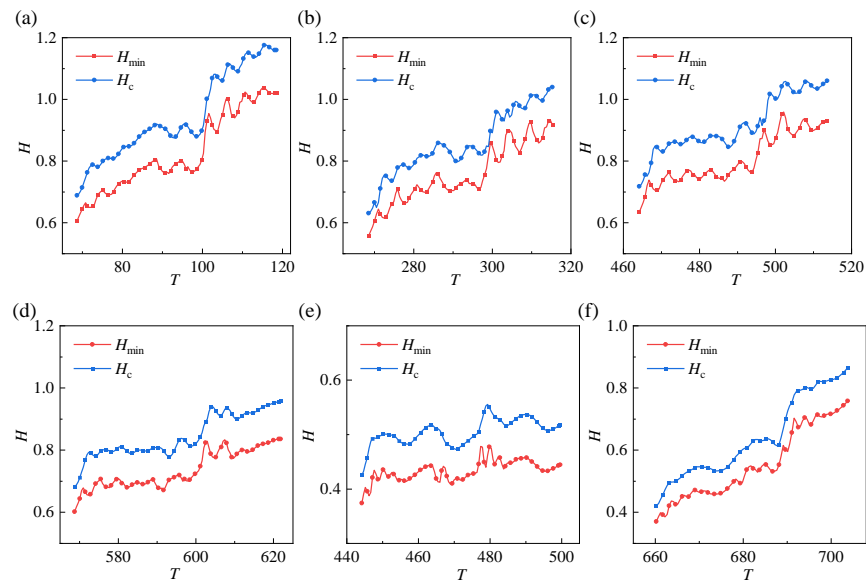


**Figure 16.** The minimum and central film thicknesses in different meshing cycles of the sin form: (a–f) six different meshing cycles.

Figure 16 depicts the minimum and central film thicknesses in different meshing cycles when the rotation speed changes in sin form. The film thickness in different meshing cycles changes periodically with the rotation speed. The range of variation in the film thickness increases with rotation speed.

#### 4. Conclusions

The dynamic response and lubrication performance of gear pairs at time-varying rotation speeds were investigated in the present work. Three time-varying rotation speed types were selected: acceleration, deceleration, and oscillation. The meshing stiffness, dynamic response, and lubrication characteristics of an involute spur gear pair were obtained. Some of the findings of this study are shown as follows:

1. The time-varying rotation speeds affect the meshing stiffness due to the variation in the rotation time per tooth. The type of time-varying rotation plays a significant role in the shape of the meshing stiffness of the gear pair.

2. The time-varying rotation speeds induce chaotic motion of the gear pair. The vibration is higher when the frequency of the rotation speed is lower, and the amplitude of the rotation speed primarily influences the fluctuation range of the dynamic transmission error.
3. The time-varying rotation speed influences the lubrication characteristics through changes in the curvature radius, entrainment velocity, and meshing force. The film thickness of each tooth is different, which makes it difficult to predict the lubricant and wear performance of the gear pair.

This study highlights the complex relationship between speed variations and dynamic behavior and lubrication performance, offering valuable insights for optimizing gear performance in variable-speed applications. The rotation speed of a given gear system not only exhibits variability but also randomness, such as for the gear pairs used in wind turbines. The models and method proposed in the paper will support dynamics and lubrication studies in the future.

**Author Contributions:** Conceptualization: J.P. and Y.T. (Yourui Tao). Methodology, J.P. Software: J.P. and H.H. Validation: Y.T. (Yuanyuan Tian) and M.W. Formal analysis: M.W. Investigation: Z.G. Resources: Y.T. (Yuanyuan Tian). Data curation: Y.T. (Yourui Tao). Writing—original draft preparation: J.P. Writing—review and editing: H.H. Visualization: Y.T. (Yuanyuan Tian). Supervision: Y.T. (Yourui Tao). Project administration: Y.T. (Yuanyuan Tian). Funding acquisition: Y.T. (Yourui Tao). All authors have read and agreed to the published version of the manuscript.

**Funding:** This work was supported by the National Natural Science Foundation of China (U23A6017, 52075146).

**Data Availability Statement:** The original contributions presented in the study are included in the article, further inquiries can be directed to the corresponding author.

**Conflicts of Interest:** The authors declare that they have no conflicts of interest.

## References

1. Özgüven, H.N.; Houser, D.R. Dynamic Analysis of High Speed Gears by Using Loaded Static Transmission Error. *J. Sound Vib.* **1988**, *125*, 71–83. [[CrossRef](#)]
2. Kahraman, A.; Singh, R. Non-linear Dynamics of a Spur Gear Pair. *J. Sound Vib.* **1990**, *142*, 49–75. [[CrossRef](#)]
3. Kahraman, A.; Blankenship, W. Interactions between commensurate parametric and forcing excit-tions in a system with clearance. *J. Sound Vib.* **1996**, *194*, 317–336. [[CrossRef](#)]
4. Kahraman, A.; Blankenship, G.W. Experiments on nonlinear dynamic behavior of an oscillator with clearance and periodically time-varying parameters. *J. Appl. Mech.* **1997**, *64*, 217–226. [[CrossRef](#)]
5. Cheng, G.; Ma, J.; Li, J.; Sun, K.; Wang, K.; Wang, Y. Study on the dynamic characteristics of gears considering surface topography in a mixed lubrication state. *Lubricants* **2024**, *12*, 7. [[CrossRef](#)]
6. Wu, S.; Zuo, M.; Parey, A. Simulation of spur gear dynamics and estimation of fault growth. *J. Sound Vib.* **2008**, *317*, 608–624. [[CrossRef](#)]
7. Yi, Y.; Huang, K.; Xiong, Y.; Sang, M. Nonlinear dynamic modelling and analysis for a spur gear system with time-varying pressure angle and gear backlash. *Mech. Syst. Signal Process.* **2019**, *132*, 18–34. [[CrossRef](#)]
8. Gharagozloo, M.; Shahmansoorian, A. Chaos control in gear transmission system using GPC and SMC controllers. *J. Appl. Comput. Mech.* **2022**, *8*, 545–556.
9. Shams, Z.; Shahmansoorian, A. Fault estimation based on observer for chaotic Lorenz system with bifurcation problem. *Trans. Inst. Meas. Control* **2020**, *42*, 576–585. [[CrossRef](#)]
10. Shi, J.; Goua, X.; Zhu, L. Modeling and analysis of a spur gear pair considering multi-state mesh with time-varying parameters and backlash. *Mech. Mach. Theory* **2019**, *134*, 582–603. [[CrossRef](#)]
11. Geng, Z.; Chen, M.; Wang, J.; Xia, Y.; Kong, Y.; Xiao, K. Nonlinear Dynamic analysis of a spur gear pair system with wear considering the meshing position. *Lubricants* **2024**, *12*, 25. [[CrossRef](#)]
12. Cao, Z.; Chen, Z.; Jiang, H. Nonlinear dynamics of a spur gear pair with force-dependent mesh stiffness. *Nonlinear Dyn.* **2020**, *99*, 1227–1241. [[CrossRef](#)]



13. Hasnijeh, S.G.; Poursina, M.; Leira, B.J.; Karimpour, H.; Chai, W. Stochastic dynamics of a nonlinear time-varying spur gear model using an adaptive time-stepping path integration method. *J. Sound Vib.* **2019**, *447*, 170–185. [[CrossRef](#)]
14. Khabou, M.T.; Bouchaala, N.; Chaari, F.; Fakhfakh, T.; Haddar, M. Study of a spur gear dynamic behavior in transient regime. *Mech. Syst. Signal Process.* **2011**, *125*, 3089–3101. [[CrossRef](#)]
15. Li, S.; Kahraman, A. A transient mixed elastohydrodynamic lubrication model for spur gear pairs. *ASME J. Tribol.* **2010**, *132*, 011501. [[CrossRef](#)]
16. Li, S.; Kahraman, A. Influence of dynamic behaviour on elastohydrodynamic lubrication of spur gears. *Proc. I. Mech. E. Part J J. Eng. Tribol.* **2011**, *225*, 740–753. [[CrossRef](#)]
17. Li, S.; Kahraman, A. prediction of spur gear mechanical power losses using a transient elastohydrodynamic lubrication model. *Tribol. Trans.* **2010**, *53*, 554–563. [[CrossRef](#)]
18. Hjelm, R.; Wahlström, J. Influence of manufacturing error tolerances on thermal EHL behavior of gears. *Lubricants* **2022**, *10*, 323. [[CrossRef](#)]
19. Xiao, Z.; Li, Z.; Shi, X.; Zhou, C. Oil film damping analysis in non-Newtonian transient thermal elastohydrodynamic lubrication for gear transmission. *J. Appl. Mech.-Trans. ASME* **2018**, *85*, 035001. [[CrossRef](#)]
20. Jamali, H.U.; Aljibori, H.S.S.; Jweeg, M.J.; Abdullah, O.I.; Ruggiero, A. An investigation on the teeth crowning effects on the transient EHL performance of large-scale wind turbine spur gears. *Lubricants* **2023**, *11*, 462. [[CrossRef](#)]
21. Liu, Y.; Gong, J. Study on TEHL flash temperature of helical gear pair considering profile modification. *Ind. Lubr. Tribol.* **2023**, *75*, 17–26. [[CrossRef](#)]
22. Huang, X.B.; Yang, B.T.; Wang, Y.Q. Influences of transient impact and vibration on the lubrication performance of spur gears. *Proc. I Mech. E. Part J J. Eng. Tribol.* **2021**, *235*, 274–289. [[CrossRef](#)]
23. Yin, Z.; Fan, Z.; Wang, M. Thermal elastohydrodynamic lubrication characteristics of double involute gears at the graded position of tooth waist. *Tribol. Int.* **2020**, *144*, 106028. [[CrossRef](#)]
24. Shi, J.; Ma, X.; Xu, C.; Zang, S. Meshing stiffness analysis of gear using the Ishikawa method. *Appl. Mech. Mater.* **2013**, *401–403*, 203–206. [[CrossRef](#)]
25. Wang, J.; He, G.; Zhang, J.; Zhao, Y.; Yao, Y. Nonlinear dynamics analysis of the spur gear system for railway locomotive. *Mech. Syst. Signal Process.* **2017**, *85*, 41–55. [[CrossRef](#)]
26. Pei, J.; Han, X.; Tao, Y.; Feng, S. Lubrication reliability analysis of spur gear systems based on random dynamics. *Tribol. Int.* **2021**, *153*, 106606. [[CrossRef](#)]
27. Larsson, R. Transient non-Newtonian elastohydrodynamic lubrication analysis of an involute spur gear. *Wear* **1997**, *207*, 67–73. [[CrossRef](#)]
28. Masjedi, M.; Khonsari, M.M. Film thickness and asperity load formulas for line-contact elastohydrodynamic lubrication with provision for surface roughness. *J. Tribol.* **2012**, *134*, 011503. [[CrossRef](#)]
29. Gu, C.; Meng, X.; Wang, S.; Ding, X. Research on mixed lubrication problems of the non-gaussian rough textured surface with the influence of stochastic roughness in consideration. *J. Tribol.* **2019**, *141*, 121501. [[CrossRef](#)]
30. Pei, J.; Han, X.; Tao, Y.; Feng, S. Mixed elastohydrodynamic lubrication analysis of line contact with non-gaussian surface roughness. *Tribol. Int.* **2020**, *151*, 106449. [[CrossRef](#)]

**Disclaimer/Publisher’s Note:** The statements, opinions and data contained in all publications are solely those of the individual author(s) and contributor(s) and not of MDPI and/or the editor(s). MDPI and/or the editor(s) disclaim responsibility for any injury to people or property resulting from any ideas, methods, instructions or products referred to in the content.